American Mineralogist, Volume 83, pages 1399–1408, 1998

Formation of Fe-silicates and Fe-oxides on bacterial surfaces in samples collected near hydrothermal vents on the Southern Explorer Ridge in the northeast Pacific Ocean

Danielle Fortin,[1,]* F. Grant Ferris,[2] and Steven D. Scott[2]

[1]Department of Geology, University of Ottawa, Ottawa, Ontario, K1N 6N6, Canada
[2] Department of Geology, E.S.C., University of Toronto, Toronto, Ontario, M5S 3B1, Canada

Abstract

Samples collected in low-temperature (2–50 °C) waters near hydrothermal vents of the Southern Explorer Ridge, in the northeast Pacific Ocean, contained fine (<500 nm) Fe- and Mn-oxide and Fe-silicate particles coating bacterial surfaces. Partially to totally mineralized bacteria, along with bacterial exopolymers, were covered with a mixture of poorly ordered Si-rich Fe-oxides (possibly ferrihydrite), Mn-oxides, and Fe-silicates (possibly nontronite). Minerals occur as very fine (2–20 nm) granular material, fine (20–100 nm) needles and sheets, small (200–500 nm) nodules and filaments (i.e., mineralized exopolymers). Under saturation conditions, we infer that bacterial surfaces provided nucleation sites for poorly ordered oxides and silicates. The formation of Fe- and Mn-oxides was likely initiated by the direct binding of soluble Fe and Mn species to reactive sites (like carboxyl, phosphate, and hydroxyl groups) present within the bacterial cell wall and the exopolymers. Fe-silicate formation involved a more complex binding mechanism, whereas metal ions, such as Fe, possibly bridged reactive sites within the cell walls to silicate anions to initiate silicate nucleation.

Introduction

Deep-sea hydrothermal vents associated with sea floor volcanism are found in many regions of the Atlantic and Pacific oceans as well as the Red Sea. As high-temperature, reducing, and acidic solutions mix with sea water, various minerals precipitate around the vents. The dominant minerals observed near hydrothermal vents are Fe-oxides (rich in Si and Mn) and Fe-sulfides, along with some sulfates, silicates, and carbonates (Juniper and Tebo 1995). Hydrothermal deposits can form not only at high temperatures near the vent openings, but also on the sea floor where the temperatures range from 2 to 50 °C (Juniper and Tebo 1995).

Hydrothermal sites are also a natural habitat for various microbial communities, such as free-living bacterial populations associated with discharged vent fluids, free-living microbial mats growing on rocks, chimneys, and sediments, endosymbiotic and exosymbiotic associations of microorganisms and vent fauna, and microorganisms within deep-sea hydrothermal vent plumes (Karl 1995). Microbial communities likely derive their energy from the oxidation of partially to fully reduced inorganic compounds, including Fe, Mn, and S, released by the vents (Karl 1995). However, no study to date has fully established a direct role (i.e., an enzymatically catalyzed reaction) for bacteria in the formation of Fe-oxides at hydrothermal vents (Juniper and Tebo 1995). Microbial Fe accumulation at these sites is therefore seen as an indirect mechanism, whereby bacteria trigger the chemical precipitation of Fe-oxides, by locally changing redox and/or pH conditions through their metabolic activity.

Bacteria can also act as nucleation surfaces for Fe-rich minerals. Bacterial surfaces can easily bind dissolved ionic species thereby leading to the nucleation of various minerals, such as oxides, silicates, carbonates, and sulfides (see review by Fortin et al. 1997). This happens because bacterial cell wall components possess amphoteric and amino groups that can sorb various ionic species, including metals (Beveridge 1981). Under solution saturation conditions, bacteria act as geochemically reactive solids (Mullen et al. 1989; Fein et al. 1997) and can, in some cases, increase the precipitation reaction rate (Fortin and Beveridge 1997).

The present study examines the morphology, chemistry, and mineralogy of Si- and Mn-rich iron oxides and Fe-silicates present in hydrothermal deposits collected near the Southern Explorer Ridge in the northeast Pacific ocean. Analyses of the deposit material by transmission electron microscopy (TEM) and energy dispersive X-ray spectroscopy (EDS) indicate that bacteria and their associated exopolymers served as nucleation surfaces for Fe-oxide and Fe-silicate formation.

Experimental details

Location

The present study was part of the CANRIDGE III investigation of ocean ridges, which is a part of the international InterRIDGE program. Samples were collected in

* E-mail: dfortin@science.uottawa.ca

0003–004X/98/1112–1399$05.00

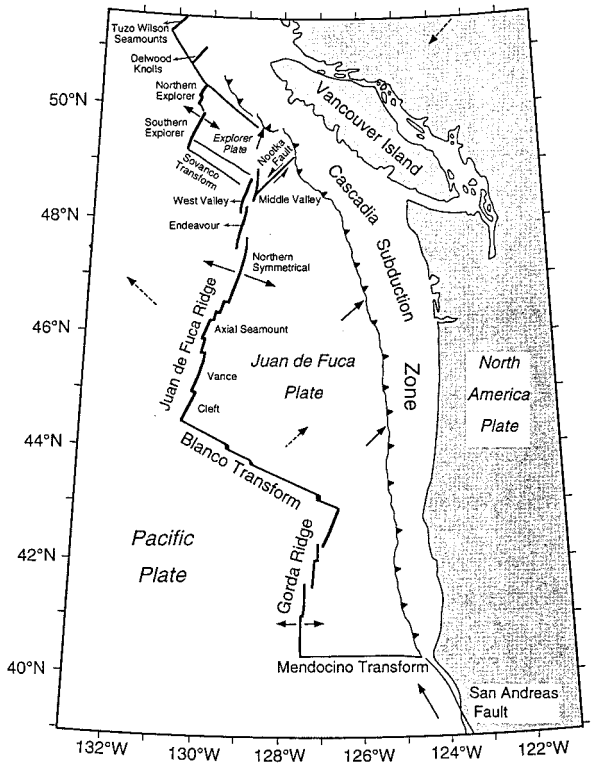

FIGURE 1. Location of the Southern Explorer Ridge west of Vancouver Island in the northeast Pacific Ocean (adapted from Davis and Currie 1993).

the summer of 1994 with the Canadian ROPOS remotely operated vehicle (ROV), at the Magic Mountain hydrothermal deposit (Southern Explorer Ridge) in the northeast Pacific Ocean (lat. 49°45′N, long. 130°27W; Fig. 1; Scott 1994).

Sampling and water analysis

Sea floor deposits (soft sediments) were taken 300 m southwest of the center of the Magic Mountain black smoker complex (at a depth of 1794 m), whereas pillow lava fragments (showing dark coatings) were taken 200 m south-southwest and 150 m southwest of the center of the complex at depths of 1808 m and 1804 m, respectively. The Magic Mountain site has been described previously by Tunnicliffe et al. (1986) and Scott et al. (1990).

Surface films and mineral crusts were recovered from rock samples by scraping ca. 2 cm^2 areas with sterile scalpels. Material removed from each rock was subsequently transferred to 10 mL plastic tubes containing 5.0 mL of 2.5% glutaraldehyde (a fixative for electron microscopy) in sea water. Water samples were analyzed on board the ship for pH and total dissolved solids (TDS) with a Corning multimeter equipped with a combination pH electrode and a conductivity probe respectively. One set of water samples was also filtered (with 0.45 μm filters) and acidified with HNO_3 (1 vol%) for elemental analysis (metals

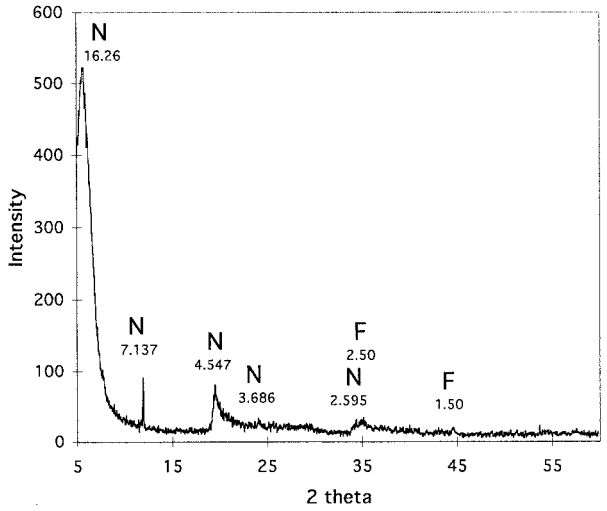

FIGURE 2. X-ray diffraction pattern of sea floor precipitates indicating the position of the main reflections (in angstroms). Nontronite = N and ferrihydrite = F.

only) by ICP-AES (XRAL Laboratories, Ontario, Canada).

Electron microscopy

Samples were prepared for TEM by dehydration in a graded series of ethanol solutions (25, 50, 75, and 100%) followed by a 50:50 ethanol:acetone and 100% acetone solutions. Each step was performed at room temperature for 15 min. The samples were then infiltrated overnight with a mixture of 50:50 acetone:Epon 812 epoxy resin (Marivac), followed by immersion in 100% resin and polymerization at 60 °C for 48 h. Thin sections were cut with a diamond knife on an Ultracut E ultramicrotome (Reichert-Jung) and collected on Formvar- and carbon-coated copper grids (Marivac). Some thin sections were stained with uranyl acetate and lead citrate solutions to enhance the contrast of bacterial structures. Thin sections were observed with a Philips EM400 electron microscope equipped with a model LZ-5 light element detector and an exL multichannel analyzer (Link analytical). EDS was

TABLE 1. General chemical composition of the water samples collected near the rock samples and typical concentrations for seawater

	Hydrothermal water	Seawater*
pH	7.15–7.66	8.20
TDS	31 g/L	35 g/L
Na	11 500 ppm	10 770 ppm
Mg	1420 ppm	1290 ppm
Ca	471–510 ppm	421 ppm
K	271–327 ppm	399 ppm
Si	3.7–5.1 ppm	1.9 ppm
P	227–343 ppb	61.8 ppb
Fe	<50 ppb	1.8 ppb
Al	<50 ppb	2.1 ppb
Mn	<5 ppb	0.2 ppb

* Stumm and Morgan (1981).

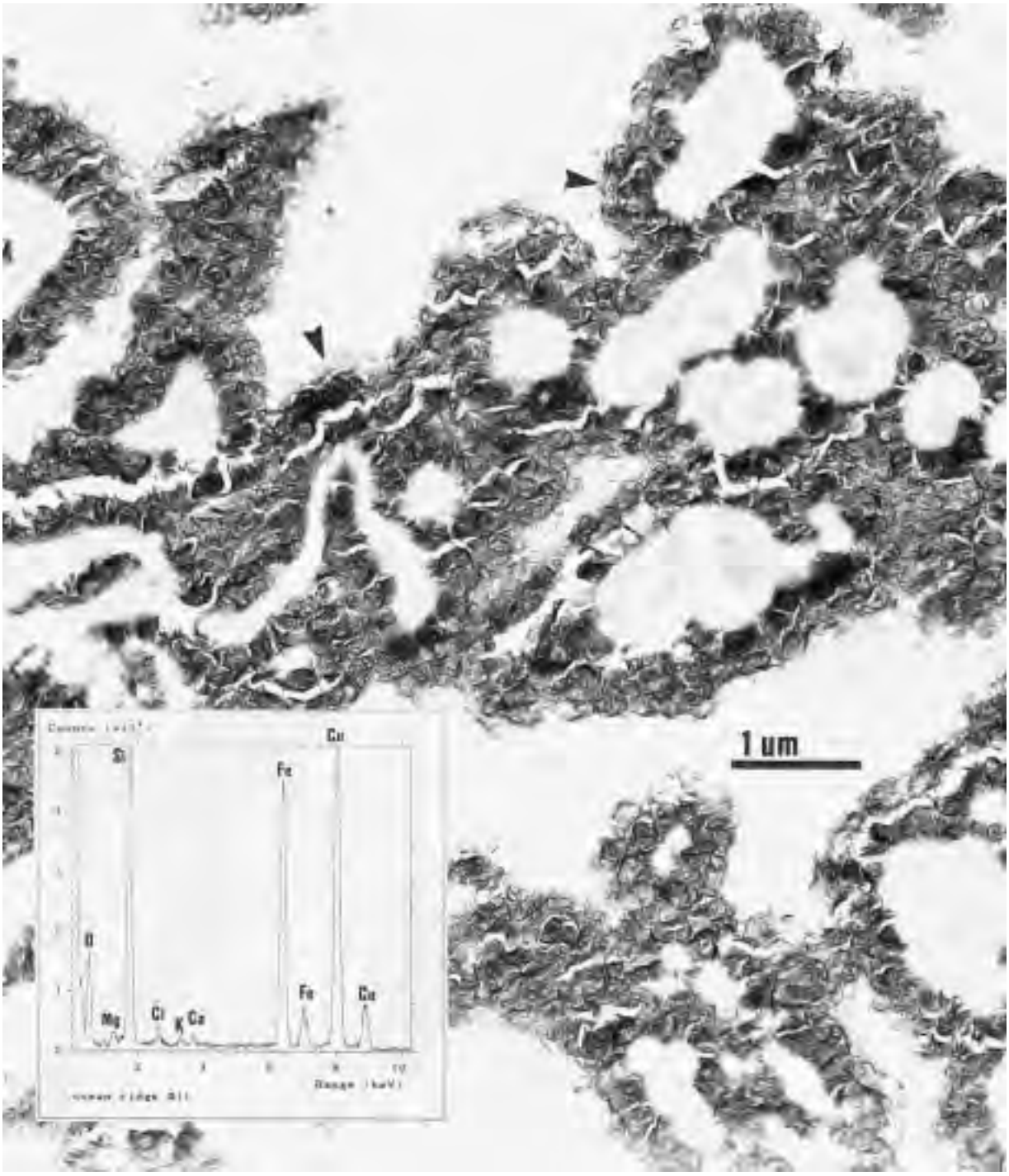

FIGURE 3. Unstained thin section of a sea floor deposit showing the presence of fine sheets aggregated around ''holes'' representing remnants of bacteria. According to EDS analysis, sheets (see arrows) showed an Fe and Si content similar to nontronite (Cu signal is from the Cu-grid).

performed at 100 kV for 100 s live time with a beam current of 0.1 μA. Selected area electron diffraction (SAED) was also performed with the same electron microscope. The accelerating voltage was 100 kV and the camera length was 640 mm.

X-ray diffraction

Approximately 1 mL of wet sample was centrifuged for 5 min at 5000 RPM in acid-washed Eppendorf tubes. The supernatant was then removed and 1 mL of ultra pure water was added. The tubes were shaken to resuspend the

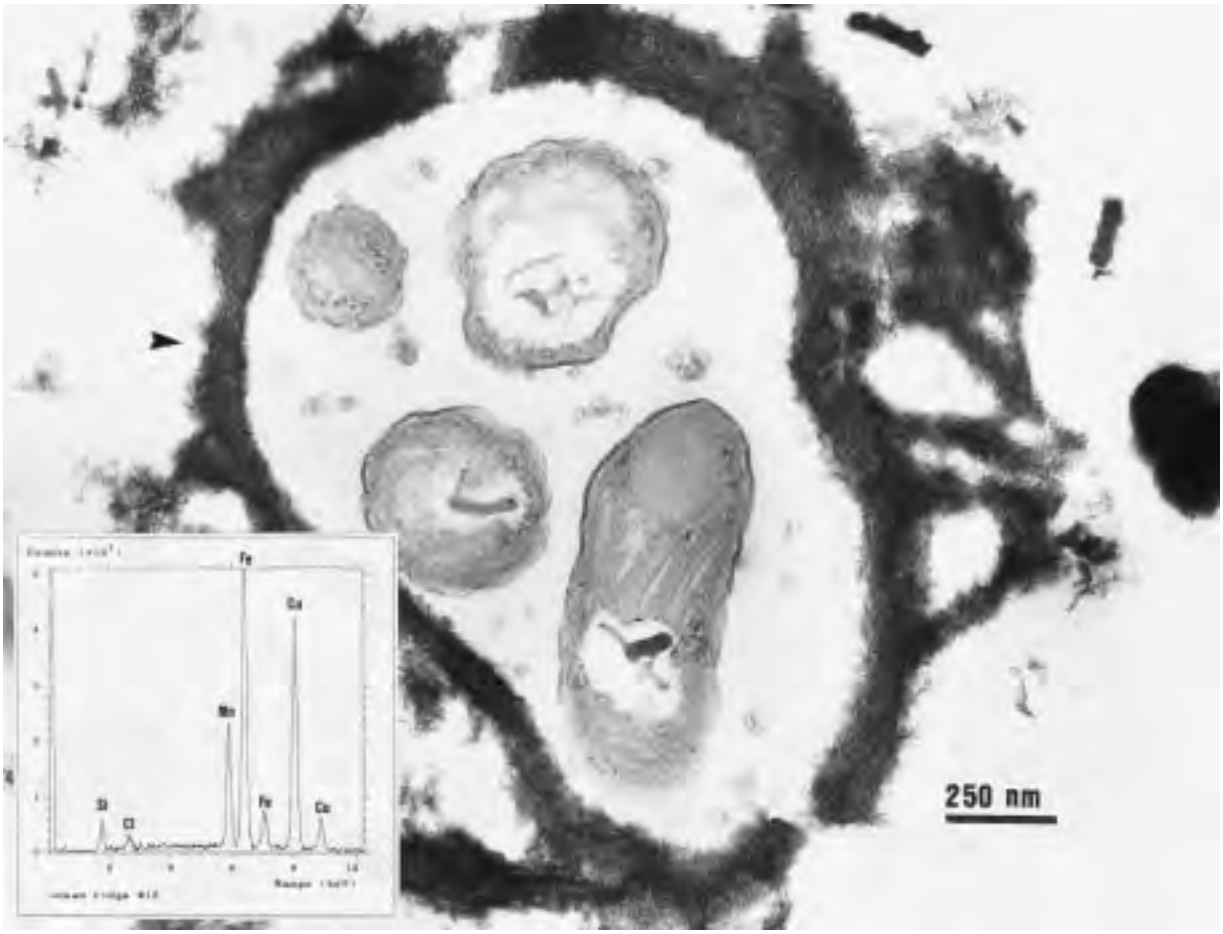

FIGURE 4. Microcolony of bacteria surrounded by very fine needles and amorphous material (see arrows) rich in Fe and Mn, with small amounts of Si and Cl (sea floor precipitate) (Cu signal is from the Cu-grid).

material and centrifuged for another 6 minutes at 6000 RPM. The supernatant was discarded and the samples were washed two more times according to the procedure outlined above. The pellets were then mixed with isopropyl alcohol and deposited on top of a Siemens low background flat sample holder, designed for very small sample amounts. X-ray diffraction (XRD) analyses were performed with a Siemens D5000 diffractometer (Dept. of Chemistry, University of Toronto, Canada), using a Cu-source operating on 50kV and 35 mA, and a Kevex Si(Li) solid-state detector. All samples were run in a step scan mode at 0.02°/1.2 s from 5 to 60 °2θ. Data were then processed by a Siemens Diffrac AT 3.1 software.

RESULTS

Samples recovered away from the active vents occurred as broken pillow lavas and precipitates on the sea floor. Pillow fragments were covered by dark to orange coatings, whereas sea floor precipitates occurred as soft orange deposits, with a green interior. XRD data indicated that sea floor precipitates were poorly crystallized, showing weak reflections characteristic of smectite-like minerals (like nontronite) and ferrihydrite (Fig. 2). Trace amounts of quartz were also observed in some samples. Samples occurring as dark coatings were amorphous (i.e., yielded no reflections). Water samples have a chemical composition similar to that of sea water, but with a lower pH and higher concentrations of Ca, Na, Mg, Si, and P, suggest some mixing with hydrothermal vent fluids (Table 1).

TEM observations of thin sections indicate the presence of very fine particles showing various morphologies. Morphological differences were not apparent between sea floor deposits and rock coatings, but coarser filaments appeared to be found mainly in rock coatings. All samples were composed of fine particulate material that was commonly dispersed around oval ''holes'' within the sections (Fig. 3). However, stained thin sections did reveal the presence of bacteria within these voids (Fig. 4). In some cases, bacterial cell walls were partially preserved through diagenetic processes (Fig. 5), but bacterial structures replaced completely by dense amorphous material in most samples (i.e., material with no apparent texture) (Fig. 5) and surrounded in many cases by more crystal-

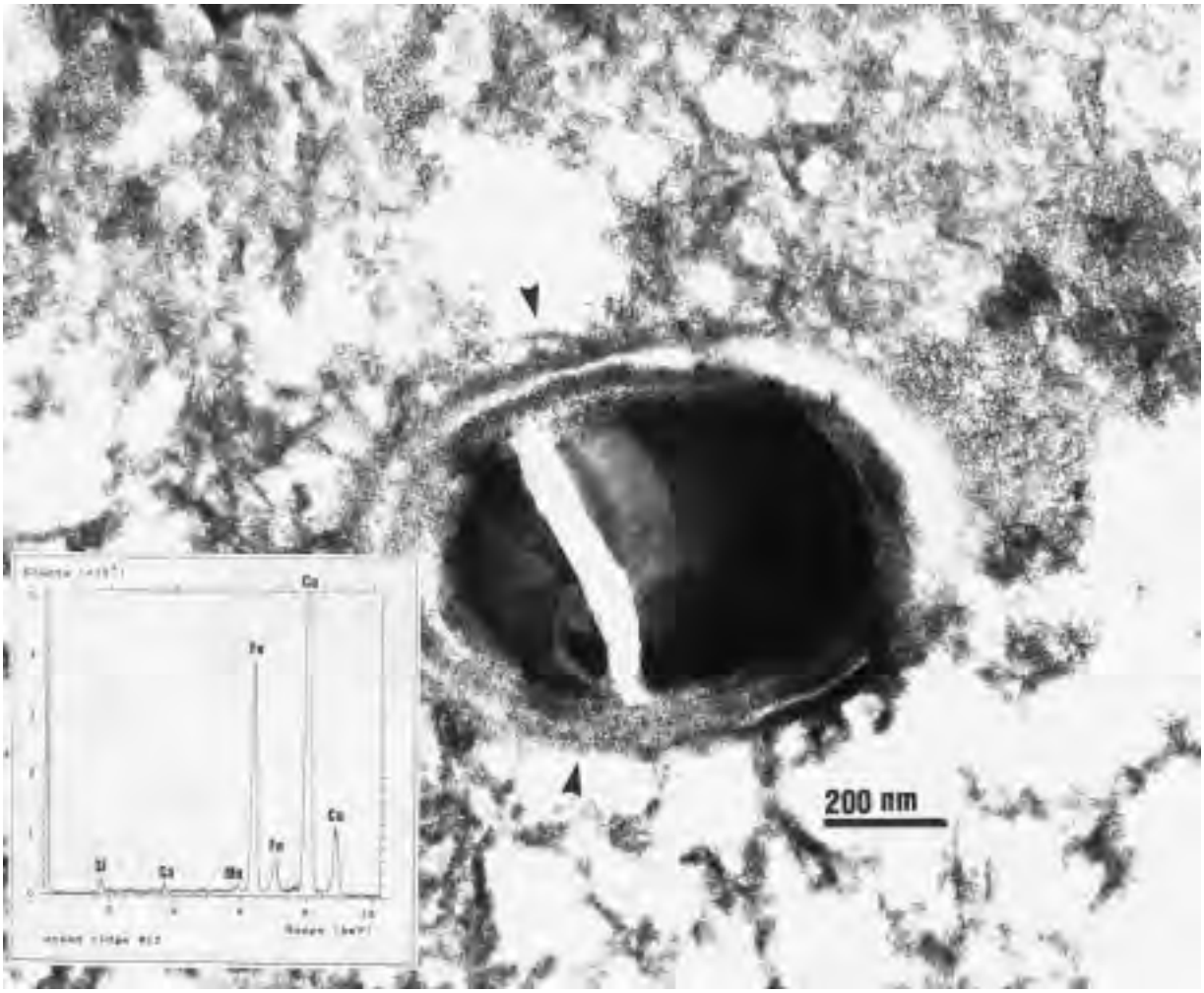

FIGURE 5. Thin section of a sea floor deposit showing a bacterium replaced completely by Fe-oxides containing some Si, Mn and Ca (see EDS spectrum). The cell wall is partially preserved and mineralized with very fine needles (see arrows), whereas the core of the bacterium is composed of amorphous Fe-rich material (the crack inside the cell is an artifact due to sectioning). (Cu signal is from the Cu-grid).

line material, such as sheets and fine needles (Fig. 6). TEM observations also revealed the presence of fine and coarse filamentous material, along with very small nodules (diam. 50–100 nm). Fine filaments commonly extended away from round ''holes'' in a reticulated network (Fig. 7), and coarser filaments appeared to be composed of linear chains of extremely small particles (diam. <20 nm; Fig. 8).

EDS analyses reveal that most amorphous and crystalline particles are composed of Fe, with variable amounts of Si (~5–65%) and some minor elements (Cl, Mg, Ca, Mn, and K). Sheets, amorphous material (Figs. 3 and 6), fine needles (mixed with amorphous material; Fig. 5), and delicate filaments (Fig. 7) are essentially composed of Fe and Si, but EDS analyses (n = 28) did not allow us to separate the various morphologies according to their respective Fe/Si ratio (Fig. 9). EDS analyses also indicated the presence of some Fe- and Mn-rich particles in the samples occurring as dark coatings. Fe and Mn are the main constituents of some amorphous material and fine needles (Figs. 4 and 5), along with coarse filaments (Fig. 8). The Mn content of amorphous (including coarse filaments) and crystalline material ranged from ~2.5 to 49% (Fig. 10). Electron diffraction analyses performed on all fine particles showed a lack of reflections or very diffuse rings, which could not be used for positive mineral identification.

DISCUSSION

Fe-rich deposits are commonly found near hydrothermal vents, but the precise mechanism of their formation remains unclear (Juniper and Tebo 1995). Results from this study do not allow confirmation of direct or indirect bacterial metabolic involvement in the formation of hydrothermal deposits, but do indicate that bacterial surfaces and their associated exopolymers acted as reactive

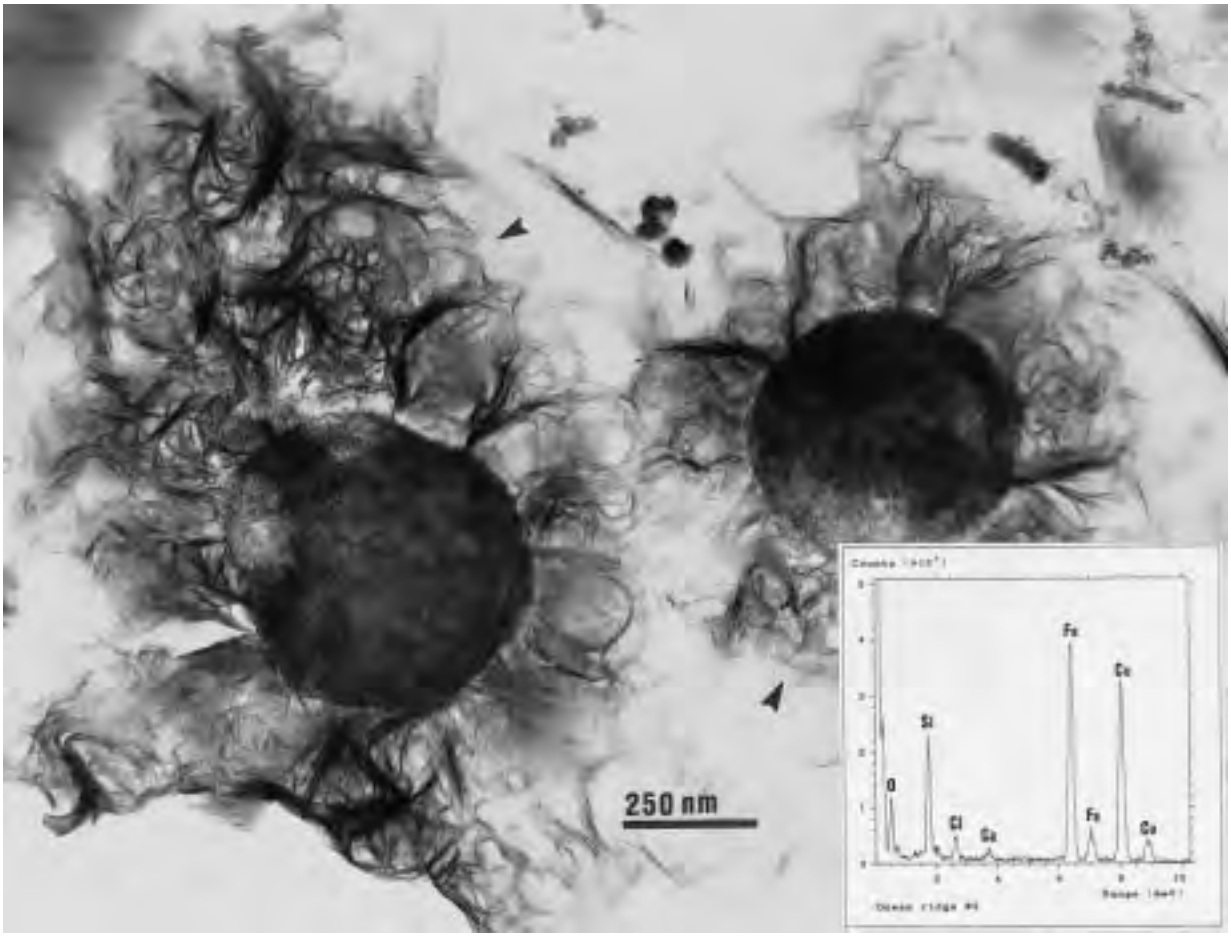

FIGURE 6. Thin section of a rock coating showing crumpled sheets (see arrows) growing on spherical nodules, possibly representing completely mineralized bacteria. EDS analyses show an identical chemical composition for the sheets and the amorphous core material, with an Fe and Si content similar to nontronite. (Cu signal is from the Cu-grid).

geochemical surfaces for mineral formation (see Figs. 3 to 8). Under neutral pH conditions, most bacteria possess an overall negative charge given by the acidic binding sites present within their cell wall components and their extracellular polymers (Beveridge 1981; 1989). Carboxyl and phosphate groups are indeed important functional groups of cell wall material, such as the peptidoglycan (the outermost layer in Gram-positive cell walls) and the outer membrane (the outermost layer in Gram-negative cell walls) (see review by Fortin et al. 1997). Carboxyl groups are also present in exopolymers.

Metal sorption to exposed carboxyl and phosphate groups in bacterial cell walls (of viable cells) fit a two-site binding model, as shown by Fein et al. (1997). Metal adsorption increases with increasing pH, indicating that metal ions are sorbed to deprotonated functional groups within the wall (Fein et al. 1997). Anion sorption to bacterial surfaces has been also shown to be responsible for mineral formation, especially silicates (Urrutia and Beveridge 1993). Silicate anions (SiO_4^{4-}) can sorb to positively charged amino groups present within the cell wall and initiate silica nucleation in pH-neutral solutions saturated with respect with silica. In the presence of metals, such as Fe, *B. subtilis* cells can also promote Fe-silicate formation (Urrutia and Beveridge 1994). These authors proposed that silicate anions (SiO_4^{4-}) sorb to negatively charged binding sites (such as carboxyl and phosphate groups) through a metal ion bridging, as a result of electrostatic interactions.

Metal and anion binding are therefore seen as the first step in mineral formation (Beveridge and Murray 1976, 1980), but mineral nucleation can be initiated only if a certain degree of oversaturation exists within the aqueous milieu surrounding the cells. At the time of formation of the samples studied here, sea water most likely was rich in metals and silicate ions, as a result of mixing with nearby hydrothermal solutions. This mixing is indeed reflected in the chemical composition of recent water samples collected near the sampling sites (Table 1).

Fe- and Mn-oxide formation

Fe-oxide formation near hydrothermal vents likely resulted from interactions between soluble Fe species and

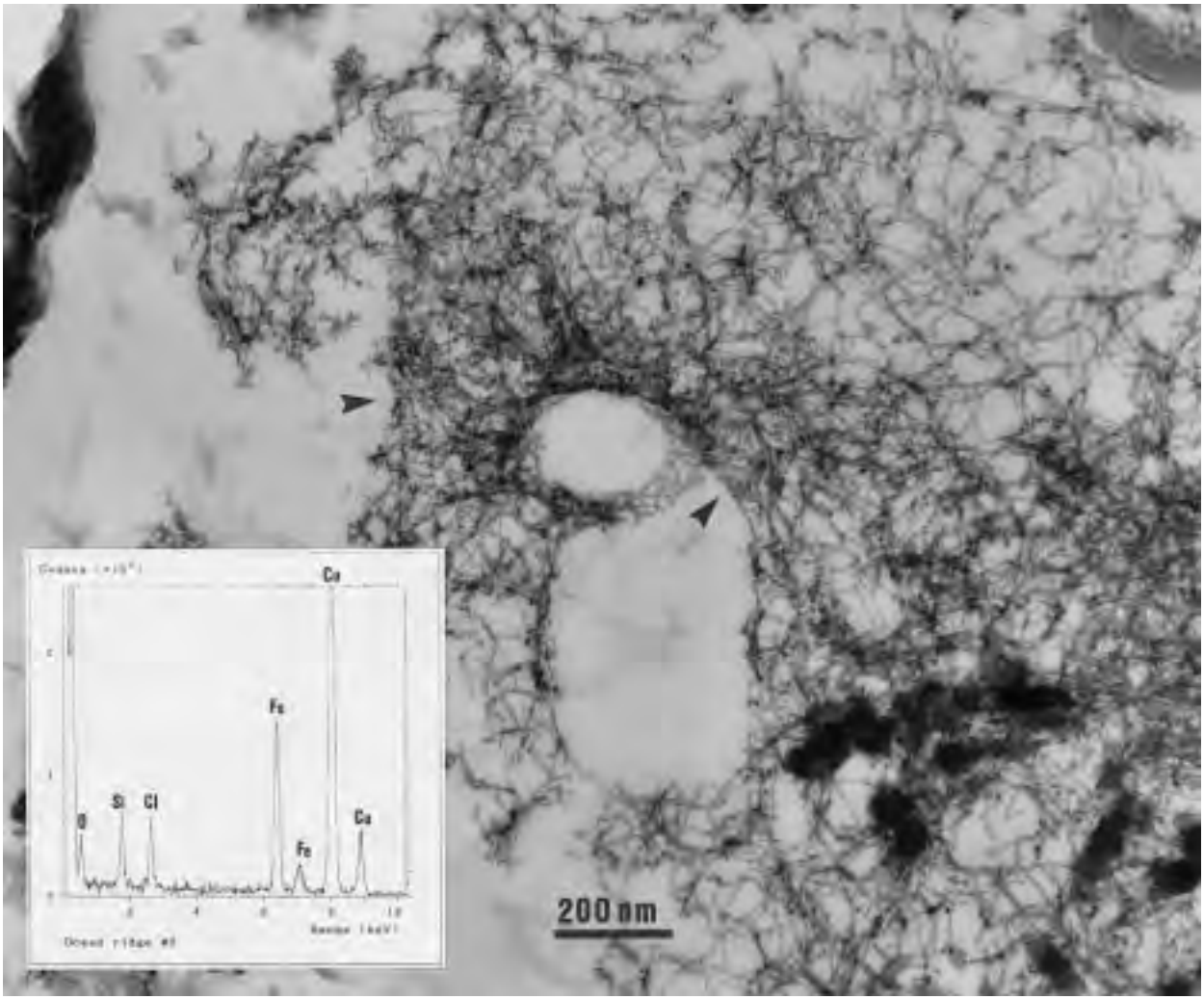

FIGURE 7. Bacterial extracellular polymers (see arrows) occurring as fine filaments of Fe-oxides containing small amounts of Si and Cl (see EDS spectrum) in a rock coating. The polymers appear to trap small round nodules also composed of Fe-oxides. (Cu signal is from the Cu-grid).

bacterial surfaces, where reactive binding sites within the cell wall and exopolymers provided nucleation sites for mineral growth. This is mostly inferred by TEM observations showing bacterial structures preserved through Fe-oxide mineralization (Figs. 5 and 7). For example, Fe-rich filaments (Figs. 7 and 8) likely represent a mass of extracellular polymers coated with Fe-oxides, as observed in other natural samples (Fortin et al. 1993; Ferris et al. 1989). Bacterial exopolymers are often produced and shed by bacterial cells. They occur as extracellular structures of 2–20 nm in diameter, having a high length-to-diameter ratio (Leppard 1986). The most commonly encountered type is a ribbon-like fibril (Leppard 1986), as shown in Figure 7.

Mineralized bacteria and polymers are not composed of pure Fe-oxide phases, EDS analyses reveal that most Fe-oxides contained variable amounts of Si and Mn (Figs. 9 and 10). Natural Fe-oxides can accommodate small amounts of Mn and Si as a result of sorption and co-precipitation reactions respectively (Fortin et al. 1993; Schwertmann and Fetcher 1982). However, the Mn contents reported here (i.e., ~2.5–49%) cannot be explained by sorption reactions, since they greatly exceed the maximum amount of Mn that can be sorbed to Fe-oxides (i.e., <1% on a molar basis; Fortin et al. 1993). This suggests that EDS signals represent a mixture of fine Fe- and Mn-oxide particles formed in close association with bacterial surfaces and exopolymers and that TEM observations could not differentiate them based on their size and morphology. It is important to mention here that the average size of individual particles was less than 10 nm, while the size of the electron beam was around 100 nm. The mineralogical composition of such mixtures remains uncertain, since XRD data indicated the presence of amorphous material.

EDS analyses also revealed that Fe-rich particles con-

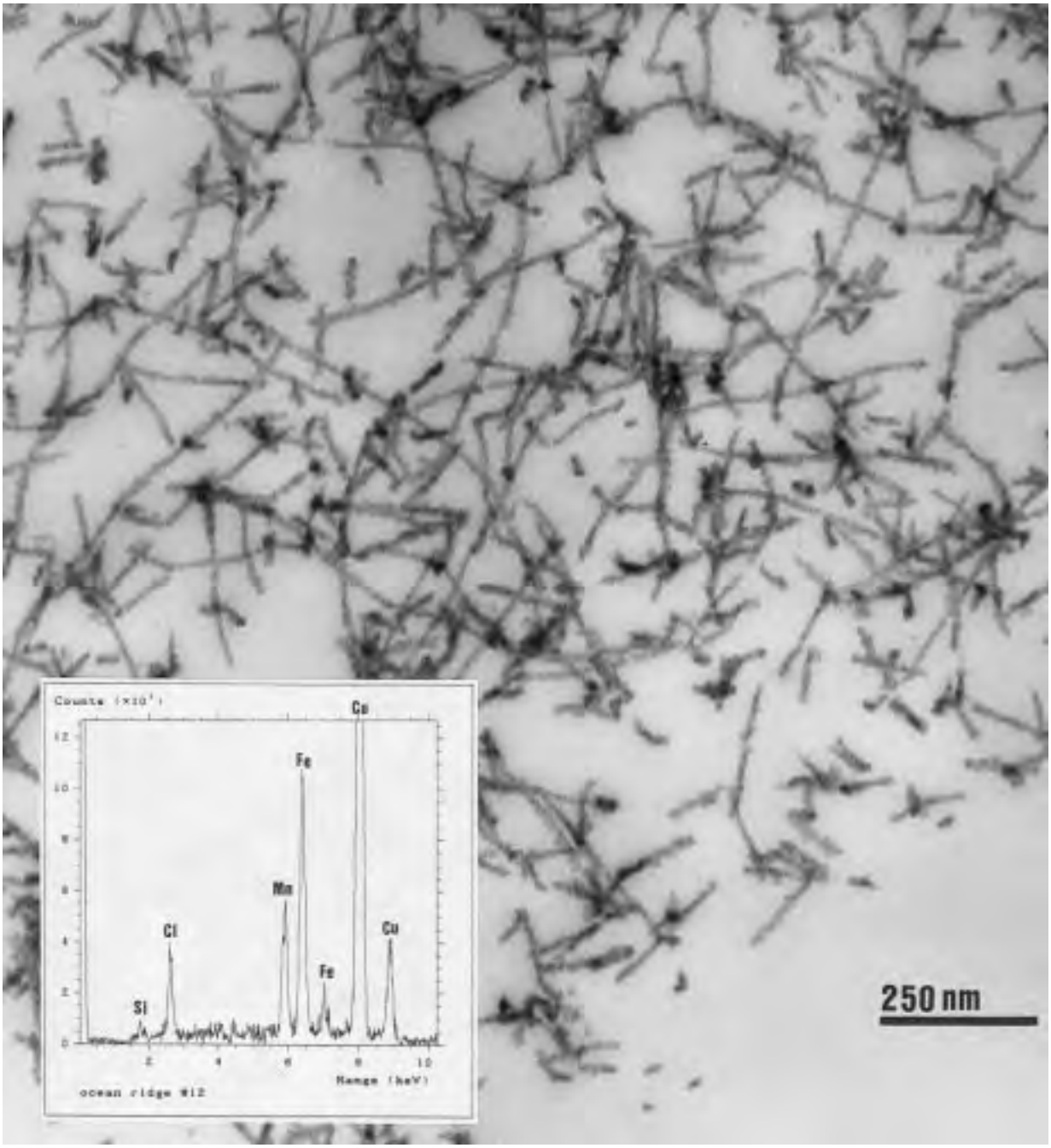

FIGURE 8. Coarse linear filaments composed of chains of very small particles mainly composed of Fe and Mn, with small amounts of Si and Cl, in a sea floor deposit. (Cu signal is from the Cu-grid).

tained variable amounts of Si (~5–65%). Most natural Fe-oxides, like ferrihydrites, can incorporate large amounts of Si (up to a maximum of 20–25% on a molar basis; Schwertmann and Fetcher 1982). From our EDS results, it is clear that not all Fe- and Si-rich particles were Fe-oxides, because many samples contained >25% Si (Fig. 9). To our knowledge, no maximum Si content has been established for natural or synthetic ferrihydrites, but it is clear that a higher Si content would change the structure of the minerals to Fe-silicates, such as nontronite, which show a Fe/Si molar ratio ranging from 0.7 to 1.0 (Manceau et al. 1995). It is also important to keep in mind that some EDS data could represent a mixture of very fine particles of Fe-oxides and Fe-silicates. Such a mixture would account for the wide range of Fe- and Si contents encountered during the EDS analyses. XRD data

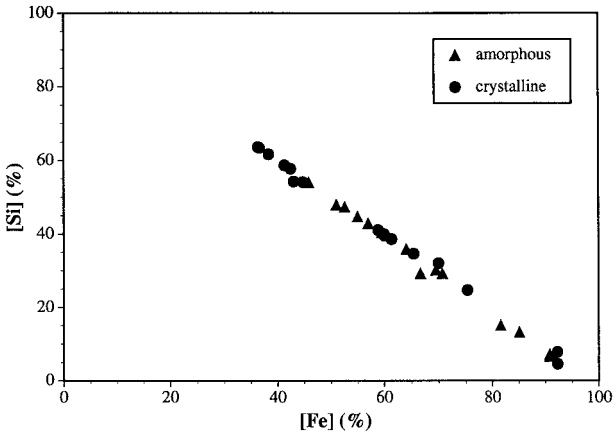

FIGURE 9. Fe and Si atomic content (%) of amorphous (including filaments) and crystalline material (i.e., sheets and needles) as determined by EDS analyses. Both amorphous and crystalline material displayed and Fe and Si content representative of both Fe-silicates (like nontronite) and Si-rich Fe-oxides (such as ferrihydrite).

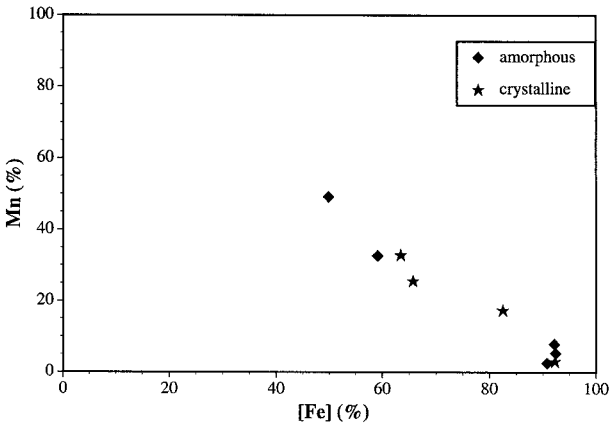

FIGURE 10. EDS analyses of amorphous (including coarse filaments) and crystalline material (fine needles) present in dark rock coatings and sea floor deposits revealed the presence of mixed Fe- and Mn-oxides and Fe-oxides containing small amounts of Mn.

(Fig. 2) do indicate that Fe-silicates, with a smectite-like structure, were present within the samples. Additionally, two weak reflections at 2.50 and 1.50 Å suggest the presence of poorly ordered ferrihydrite. Our X-ray and electron diffraction analyses remain inconclusive regarding the definite crystalline composition of the particles, but do support the EDS data, which indicate that both Fe-silicates and Fe-oxides are present within the samples. The presence of small amounts of Si in the iron oxides would also explain their poorly ordered nature, because Si affects the growth of more crystalline Fe-oxide, such as lepidocrocite (Schwertmann and Taylor 1979) thereby preventing any further transformation into more crystalline phases (Vempati and Loeppert 1989).

Fe-silicate formation

Fe-silicates were observed in close association with bacteria (Figs. 3 and 6), where they occurred as sheets or amorphous material. The observation that silicate sheets are ''rooted'' in the cell surface (Fig. 6) strongly suggests that the cell wall served as a nucleation surface for mineral formation, and not that clay minerals formed first in solution and then sorbed to the surface of the cell. Silicate formation on bacterial surfaces has been reported in various environments, such as hot-springs (Schultze-Lam et al. 1995; Ferris et al. 1986), river sediments and biofilms (Konhauser et al. 1993, 1994), and mine tailings (Ferris et al. 1987; Fortin and Beveridge 1997). Those studies reported the presence of amorphous silica, poorly ordered chamositic clays, and more crystalline silicates, such as kaolinite and glauconite-like minerals, all of which formed as a result of the interactions between binding sites within the bacterial cell walls and soluble metal species and silicate anions. Smectite-type minerals have often been reported in hydrothermal deposits, but their mechanism(s) of formation remains unclear (Juniper and Tebo 1995; Juniper and Fouquet 1988; Rona 1988). As mentioned earlier, a direct or indirect metabolic role is difficult to assess in the present case because most samples were highly mineralized and contained no live bacteria. According to TEM observations, it appears that bacterial surfaces acted as passive nucleation surfaces for smectite-type mineral formation. The chemical composition (i.e., Fe/Si ratio) and shape of the minerals changed over time, suggesting changes in the solution chemistry (Fig. 6). It is probable that silicate formation was initiated by Fe^{3+} species bridging negatively charged binding sites within the cell wall and silicate anions, as reported by Urrutia and Beverige (1994). Direct binding of silicate anions to amino groups appears unlikely, because hydrothermal solutions were rich in metals (such as Fe and Mn) and that bacteria possess more negative sites than positive ones within their wall.

Mineralization near and at hydrothermal sea vents remains an active research subject in Earth science today. Fe- and Mn-oxide and silicate precipitation have often been reported in those environments, but the mechanism that controls their formation, especially away from the vents, still triggers a debate. Are bacteria catalyzing the precipitation reactions? The present research does not answer those questions, but does indicate that bacteria, when present in low-temperature environments near hydrothermal vents, can easily nucleate a variety of minerals.

ACKNOWLEDGMENTS

This work was supported by the Natural Science and Engineering Research Council of Canada (NSERC). The authors also thank B. Harris and T.J. Beveridge of the University of Guelph, Canada.

REFERENCES CITED

Beveridge, T.J. (1981) Ultrastructure, chemistry and function of the bacterial wall. International Review of Cytology, 72, 229–317.

———(1989) The structure of bacteria. In J.S. Poindexter and E.R. Leadbetter, (Eds.), Bacteria in Nature, Plenum Press, New York, 1–65.

Beveridge, T.J. and Murray, R.G.E. (1976). Uptake and retention of metals by cell walls of Bacillus subtilis. Journal of Bacteriology, 127, 1502–1518.

———(1980). Sites of metal deposition in the cell wall of Bacillus subtilis. Journal of Bacteriology, 141, 876–887.

Davis, E.E. and Currie, R.G. (1993) Geophysical observations of the northern Juan de Fuca Ridge system: lessons in sea-floor spreading. Canadian Journal of Earth Sciences, 30, 278–300.

Fein, J.B., Daughney, C.J., Yee, N., and Davis, T.A. (1997). A chemical equilibrium model for metal adsorption onto bacterial surfaces. Geochimica Cosmochimica Acta, 61, 3319–3328.

Ferris, F.G., Beveridge, T.J., and Fyfe, W.S. (1986) Iron-silica crystallite nucleation by bacteria in a geothermal sediment. Nature, 320, 609–611.

Ferris, F.G., Fyfe, W.S., and Beveridge, T.J. (1987) Bacteria as nucleation sites for authigenic minerals in a metal contaminated lake sediment. Chemical Geology, 63, 225–232.

Ferris, F.G., Schultze, S., Witten, T., Fyfe, W.S., and Beveidge, T.J. (1989). Metal interactions with microbial biofilms in acidic and neutral pH environments. Applied and Environmental Microbiology, 55, 1249–1257.

Fortin, D. and Beveridge, T.J. (1997) Role of the bacterium, Thiobacillus, in the formation of silicates in acidic mine tailings. Chemical Geology, 141, 235–250.

Fortin, D., Leppard, G.G., and Tessier, A. (1993). Characteristics of lacustrine diagenetic iron oxyhydroxides. Geochimica Cosmochimica Acta, 57, 4391–4404.

Fortin, D., Ferris, F.G., and Beveridge, T.J. (1997) Surface-mediated mineral development by bacteria. In Mineralogical Society of America Reviews in Mineralogy, 35, 161–180.

Juniper, S.K. and Fouquet, Y. (1988) Filamentous Iron-Silica deposits from modern and ancient hydrothermal sites. Canadian Mineralogist, 26, 859–869.

Juniper, S.K. and Tebo, B.M. (1995) Microbe-metal interactions and mineral deposition at hydrothermal vents, In D.M. Karl, (Ed.), The Microbiology of Deep-Sea Hydrothermal Vents, p. 219–253. CRC Press, New York.

Karl, D.M. (1995) Ecology of free-living, hydrothermal vent microbial communities. In D.M. Karl, (Ed.), The Microbiology of Deep-Sea Hydrothermal Vents, p. 219–253. CRC Press, New York.

Konhauser, K.O., Fyfe, W.S., Ferris, F.G., and Beveridge, T.J. (1993). Metal sorption and mineral precipitation by bacteria in two Amazonian river systems: Rio Solimoes and Rio Negro, Brazil. Geology, 21, 1103–1106.

Konhauser, K.O., Scultze-Lam, S., Ferris, F.G., Fyfe, W.S., Longstaff, F.J., and Beveridge, T.J. (1994) Mineral precipitaiton by epilithic biofilms in the Speed river, Ontario, Canada. Applied and Environmental Microbiology, 60, 549–553.

Leppard, G.G. (1986) The fibrillar matrix component of lacustrine biofilms. Water Ressources, 20, 697–702.

Manceau, A., Ildefonce, P.H., Hazemann, J.L., Flank, A-M., and Gallup, D. (1995). Crystall chemistry of hydrous iron silicate scale deposits at the Salton Sea geothermal field. Clays and Clay Minerals, 43, 304–317.

Mullen, M.D., Wolf, D.C., Ferrris, F.G., Beveridge, T.J., Flemming, C.A., and Bailey, G.W. (1989) Bacterial sorption of heavy metals. Applied and Environmental Microbiology, 55, 3143–3149.

Scott, S.D. (1994) ROPOS ROV operations at the Southern Explorer Ridge during the July 1994 CANRIDGE III cruise. EOS Transactions, American Geophysics Union Abstracts, p. 312.

Scott, S.D., Chase, R.L., Hannington, M.D., Michael, P.J., McConachy, T.F., and Shea, G.T. (1990). Sulfide deposits, tectonics and petrogenesis of Explorer Ridge, northeast Pacific Ocean. In J. Malps et al., (Eds.), Ophiolites: Oceanic crustal analogs, Proceedings of the Symposium in Troodos 1997. Geological Survey Department, Nicosia, 719–733.

Rona, P.A. (1988) Hydrothermal mineralization at oceanic ridges. Canadian Mineralogist, 26, 431–465.

Schultze-Lam, S., Ferris, F.G., Konhauser, K.O., and Wiese, R.G. (1995) In situ silicification of an Icelandic hot spring microbial mat: implications for microfossil formation. Canadian Journal of Earth Sciences, 32, 2021–2026.

Schwertmann, U. and Fetcher, H. (1982). The point of zero point of charge of natural and synthetic ferrihydrites and its relation to adsorbed silicate. Clay Minerals, 17, 471–476.

Schwertmann, U. and Taylor, R.M. (1979). Natural and synthetic poorly crystallized lepidocrocite. Clay Minerals, 14, 285–293.

Stumm, W. and Morgan, J.J. (1981) Aquatic Chemistry. 2nd Ed, Wiley, New York.

Tunnicliffe, U., Botros, M., Deburgh, M.E., Dinet, A., Johnson, H.P., Juniper, S.K., and McDuff, R.E. (1986) Hydrothermal vents of the Explorer region, northeast Pacific. Deep Sea Research, 33, 401–412.

Urrutia, M.M. and Beveridge, T.J. (1993) Mechanism of silicate binding to the bacterial cell wall in Bacillus subtilis. Journal of Bacteriology, 175, 1936–1945.

———(1994) Formation of fine-grained silicate minerals and metal precipitates by a bacterial surface (Bacillus subtilis) and the implications in the global cycling of silicon. Chemical Geology, 116, 261–280.

Vempati, R.K. and Loeppert, R.H. (1989) Influence of structural and adsorbed Si on the transformation of synthetic ferrihydrite. Clays and Clay Minerals, 37, 272–279.

Manuscript received February 9, 1998
Manuscript accepted August 4, 1998
Paper handled by Jillian F. Banfield